Trinuclear copper biocatalytic center forms an active site of thiocyanate dehydrogenase

Tikhonova, Tamara V.; Sorokin, Dimitry Y.; Hagen, Wilfred R.; Khrenova, Maria G.; Muyzer, Gerard; Rakitina, Tatiana V.; Shabalin, Ivan G.; Trofimov, Anton A.; Tsallagov, Stanislav I.; Popov, Vladimir O.

DOI
10.1073/pnas.1922133117

Publication date
2020

Document Version
Final published version

Published in
Proceedings of the National Academy of Sciences of the United States of America

Trinuclear copper biocatalytic center forms an active site of thiocyanate dehydrogenase

Tamara V. Tikhonova[a,1], Dimitry Y. Sorokin[a,b,1], Wilfred R. Hagen[b], Maria G. Khrenova[a,c], Gerard Muyzer[d], Tatiana V. Rakitina[e,f], Ivan G. Shabalin[g], Anton A. Trofimov[h], Stanislav I. Tsallagov[a], and Vladimir O. Popov[a,f,2]

[a]Research Centre of Biotechnology, Russian Academy of Sciences, 119071 Moscow, Russia; [b]Department of Biotechnology, Delft University of Technology, Delft, 2629 HZ The Netherlands; [c]Department of Chemistry, Lomonosov Moscow State University, 119991 Moscow, Russia; [d]Department of Freshwater and Marine Ecology, Institute for Biodiversity and Ecosystem Dynamics, University of Amsterdam, Amsterdam, 1098 XH The Netherlands; [e]Shemyakin-Ovchinnikov Institute of Bioorganic Chemistry, Russian Academy of Sciences, 117997 Moscow, Russia; [f]Kurchatov Complex NBICS-Technologies, National Research Center "Kurchatov Institute", 123182 Moscow, Russia; [g]Department of Molecular Physiology and Biological Physics, University of Virginia, Charlottesville, VA 22903; and [h]Engelhardt Institute of Molecular Biology, Russian Academy of Sciences, 119991 Moscow, Russia

Edited by Edward I. Solomon, Stanford University, Stanford, CA, and approved January 27, 2020 (received for review December 29, 2019)

Biocatalytic copper centers are generally involved in the activation and reduction of dioxygen, with only few exceptions known. Here we report the discovery and characterization of a previously undescribed copper center that forms the active site of a copper-containing enzyme thiocyanate dehydrogenase (suggested EC 1.8.2.7) that was purified from the haloalkaliphilic sulfur-oxidizing bacterium of the genus *Thioalkalivibrio* ubiquitous in saline alkaline soda lakes. The copper cluster is formed by three copper ions located at the corners of a near-isosceles triangle and facilitates a direct thiocyanate conversion into cyanate, elemental sulfur, and two reducing equivalents without involvement of molecular oxygen. A molecular mechanism of catalysis is suggested based on high-resolution three-dimensional structures, electron paramagnetic resonance (EPR) spectroscopy, quantum mechanics/molecular mechanics (QM/MM) simulations, kinetic studies, and the results of site-directed mutagenesis.

copper centers | thiocyanate dehydrogenase | crystal structure | EPR | molecular mechanism

Copper is widely utilized in life systems (1, 2). It is incorporated into proteins for the purposes of copper trafficking and storage (3, 4) and electron transport and catalysis (5–7). Malfunctioning of copper homeostasis leads to a number of disease states (8, 9). Copper enzymes are important in the biosynthesis of natural products, hormones and neurotransmitters, proton pumping for adenosine triphosphate synthesis, and the metabolism of iron and copper (1, 2). They are also of potential technological interest for construction of the anodes of (implantable) biofuel cells (10).

Copper enzymes comprise a rather diverse, but not numerous, group of biocatalysts. Over 20 copper-containing enzymes that catalyze a wide-ranging group of chemical reactions have been characterized so far (1, 2). With just a few exceptions [enzymes participating in nitrogen metabolism, nitrite reductase (11) and nitrous oxide reductase (12), and lytic polysaccharide monooxygenase (13) thought to utilize peroxide as an oxidant], all of the other Cu-based biocatalysts use dioxygen as a reactant. With the help of copper proteins, dioxygen is activated for the monooxygenation, dioxygenation, or oxidation of substrate molecules, and can also undergo four-electron reduction to water.

Copper-dependent catalysis resides on the redox properties of the Cu^{2+}/Cu^{+} couple and geometry and electronic structures of the individual Cu-sites (1, 2). Quite a few Cu-centers that differ in the number and geometry of the constituent copper atoms are known to date. Enzyme active centers were reported to contain metal clusters comprising one to four copper ions as well as other moieties such as heme groups (14–16).

Thiocyanate is a relatively stable compound and is oxidized by dioxygen only under elevated temperatures and pressures (up to 200 °C and 100 bar) in the presence of Cu(II) catalyst (17). According to a suggested mechanism (17), the process proceeds via initial formation of $(NCS)_2Cu$, comprises multiple stages, and gives sulfate as the final sulfur reaction product. Some sulfur-oxidizing bacteria (SOB) known to play an important role in global geochemical cycles can utilize thiocyanate as the sole source of energy and nitrogen. Until now, the only route of thiocyanate microbial utilization that has been documented involved the hydrolytic cleavage of nitrile, leading to formation of carbonyl sulfide and ammonia (18–20). However, some previous microbiological evidence showed that thiocyanate may be degraded by cell-free extracts of haloalkaliphilic thiocyanate-utilizing SOB in the presence of an electron acceptor via a chemical reaction producing cyanate and elemental sulfur as final products (21, 22):

$$N \equiv C\text{-}S^- + H_2O \rightarrow N \equiv C\text{-}O^- + S^0 + 2H^+ + 2e^- \qquad [1]$$

Here we present firm evidence that a specific enzyme from the haloalkaliphilic SOB of the genus *Thioalkalivibrio* can catalyze this process. The enzyme, thiocyanate dehydrogenase (TcDH), reveals several features special to the chemistry of biological copper sites. TcDH contains a unique metal site comprising three copper ions in a configuration that enables two-electron oxidation of thiocyanate ion to cyanate and elemental sulfur

Significance

The bioinorganic chemistry of copper is currently confined to a few mononuclear and polynuclear clusters in less than two dozen different types of enzymes catalyzing diverse biological reactions. Here we present an unpreviously reported type of a polynuclear center consisting of three copper ions, which form the active site of a not previously described enzyme, thiocyanate dehydrogenase. Enzymatic thiocyanate degradation resides on the copper cluster and proceeds via a chemical reaction unmatched in the chemistry of thiocyanate. Our findings expand the knowledge on copper-containing enzymes and reveal a catalytic machinery employing a trinuclear copper center.

Author contributions: T.V.T., D.Y.S., and V.O.P. designed research; W.R.H., M.G.K., G.M., T.V.R., I.G.S., A.A.T., and S.I.T. performed research; T.V.T., D.Y.S., W.R.H., M.G.K., S.I.T., and V.O.P. analyzed data; and V.O.P. wrote the paper.

The authors declare no competing interest.

This article is a PNAS Direct Submission.

Data deposition: The atomic coordinates and structure factors have been deposited in the Protein Data Bank, http://www.wwpdb.org/ (PDB ID codes 6I3Q, 6UWE, 6SJI, and 6G50).

[1]T.V.T. and D.Y.S. contributed equally to this work.

[2]To whom correspondence may be addressed. Email: vpopov@inbi.ras.ru.

This article contains supporting information online at https://www.pnas.org/lookup/suppl/doi:10.1073/pnas.1922133117/-/DCSupplemental.

First published February 24, 2020.

without utilizing oxygen as a cosubstrate. We describe physicochemical and catalytic properties of TcDH, solve and characterize its three-dimensional structure, provide data on the electronic state of the copper cluster, and propose and verify a possible molecular mechanism of action.

Results and Discussion

Isolation and Characterization of TcDH.

Thiocyanate-utilizing potential within the genus **Thioalkalivibrio.** Haloalkaliphilic sulfur-oxidizing bacteria of the genus *Thioalkalivibrio* can utilize sulfide, sulfur, or thiosulfate as energy sources during aerobic growth. The strains used in this study, *Thioalkalivibrio paradoxus* (ARh1) and *Thioalkalivibrio thiocyanoxidans* (ARh2 and ARh4) (21, 22), can grow using thiocyanate as the sole source of energy and nitrogen.

For all of the three strains tested, polypeptide profiles of cells grown with either thiosulfate or thiocyanate as an energy source showed a major protein with a molecular weight of ∼52 to 55 kDa unique to thiocyanate-grown cells (*SI Appendix*, Fig. S1*A*). An increase in the copper concentration in the growth medium correlated both with an increase in the accumulation of this protein in cell extracts (*SI Appendix*, Fig. S1*B*) and an increase in the thiocyanate consumption and biomass accumulation rate (*SI Appendix*, Fig. S2*A*). In contrast, copper ions had no effect when cells were grown on thiosulfate (*SI Appendix*, Fig. S2*B*), further verifying their specific influence on the primary thiocyanate degradation reaction.

Putative thiocyanate-degrading enzymes were isolated from the soluble fractions of cell homogenates of the ARh1 and ARh4 strains and were purified to homogeneity. The proteins were identified by matrix assisted laser desorption/ionization - time-of-flight (MALDI-TOF) mass spectrometry as products of the THITH_RS12920 and F465DRAFT_2664 genes in the genomes *Tv. paradoxus* ARh1 and *Tv. thiocyanoxidans* ARh4, respectively. An analysis of 75 annotated genomes of the strains belonging to the genus *Thioalkalivibrio* demonstrated that genes encoding homologous proteins (88.9 to 94% identity) are present in the genomes of 10 bacteria (23) (*SI Appendix*, Table S1). Further examination showed that all of the strains of the genus *Thioalkalivibrio* that contain the gene encoding the thiocyanate-degrading protein are able to grow aerobically with thiocyanate as an energy source (*SI Appendix*, Fig. S2*C*). Proteins homologous to TcDH (sequence identity above 30%) were found in the genomes of more than 50 other species from phylogenetically different bacteria (24).

The thiocyanate-degrading enzyme from *Tv. paradoxus* ARh1 was selected for further detailed characterization.

Molecular properties and functional characterization of the thiocyanate-degrading enzyme. The target protein was isolated from the periplasmic cell fraction and purified to homogeneity by anion-exchange and size-exclusion chromatography. The isolation led to a decrease in the specific activity of the target protein due to loss of copper ions (as detailed later) required for enzyme activity (*SI Appendix*, Table S2). N-terminal sequencing demonstrated that the mature form of the target protein begins at residue Ser79. The calculated molecular weight of the mature protein is 51,891 Da, in agreement with the protein mass determined from SDS/PAGE (52 to 53 kDa). According to size-exclusion chromatography results, the native enzyme exists as a dimer in solution at pH 9 to 10 (25 mM borate or carbonate buffer) in the presence of 0.15 to 1 M NaCl. The protein has no characteristic absorption in the visible region. An X-ray fluorescence study demonstrated that the "as-isolated" protein contained significant amounts of copper ions (0.6 to 0.9 moles per mole of protein subunit).

The reaction of thiocyanate oxidation proceeded only in the presence of electron acceptors with potentials E_0' higher than 200 mV, such as endogenous periplasmic cytochromes, horse heart cytochrome *c550*, Wurster's blue, Bindschedler's green, and $K_3Fe(CN)_6$. Low-potential electron acceptors, such as 2,3,5-triphenyltetrazolium chloride and methylene blue, were not reduced. Direct oxidation of thiocyanate by molecular oxygen was not observed.

The degradation of thiocyanate was accompanied by the formation of one equivalent of cyanate and the reduction of two equivalents of one-electron acceptors (ferricyanide, *c550*; *SI Appendix*, Fig. S3). The formation of elemental sulfur as the second product of the thiocyanate oxidation was confirmed by reversed-phase high-performance liquid chromatography (HPLC) using biosulfur from *Tv. paradoxus* ARh1 as a marker (*SI Appendix*, Fig. S4) (25).

These results show that the thiocyanate-degrading enzyme catalyzes the two-electron oxidation of thiocyanate to yield cyanate and elemental sulfur, coupled with electron transfer to an external electron acceptor (cytochromes), and is thus a thiocyanate: cytochrome c oxidoreductase (or thiocyanate dehydrogenase, TcDH). According to the Enzyme Commission (EC) classification, TcDH can be assigned to the ENZYME class 1.8.2., which includes oxidoreductases acting on a sulfur group of donors using cytochrome as an acceptor.

Influence of copper ions on TcDH activity. The "as-isolated" TcDH demonstrated low activity and contained 0.6 to 0.9 copper ions per enzyme subunit, depending on the isolation protocol. Exhaustive dialysis against 25 mM borate buffer, pH 9.5, containing 10 mM EDTA, did not lead to a substantial decrease in copper content, while the TcDH activity further decreased to 3% of the "as-isolated" value (Table 1).

Incubation of the "as-isolated" TcDH with 20 to 40 molar excess of the copper salts for 1 to 2 h resulted in the binding of copper ions and concomitant increase in specific activity of TcDH (Table 1). TcDH sample saturated with Cu^{2+} ions (hereafter referred to as "Cu^{2+}-saturated") contains 3.0 ± 0.5 copper ions per enzyme subunit as revealed by inductively coupled plasma-mass spectrometry (ICP-MS) metal analysis. The activation of the enzyme by Cu^{+} ions yielded only slightly higher results but consistently higher copper incorporation (Table 1). The reasons for the latter phenomenon are discussed later.

Taken together, these data suggest that each subunit of "as-isolated" TcDH contains one strongly bound copper ion that is not lost during the isolation procedure and does not dissociate during dialysis. Exhaustive dialysis provided evidence that TcDH containing one copper ion has no catalytic activity. The activity of "as-isolated" TcDH observed in our experiments is apparently attributable to the presence of a small amount (3 to 5%) of the catalytically active form containing three copper ions per protein molecule. It can be hypothesized that the incubation with copper salts allows for the incorporation of copper ions into the TcDH molecule that were lost during the isolation procedure.

Experiments with recombinant TcDH (recTcDH) support this assumption. When purified, recTcDH contains no metal ions and is devoid of catalytic activity. However, similar to the wild-type protein, it can be reactivated by copper ions with subsequent reconstitution of the catalytic activity (Table 1).

The key role of copper ions in the functioning of TcDH is additionally confirmed by the enhanced TcDH biosynthesis and increased rate of thiocyanate consumption by cells grown under increased copper concentration in the growth media (*SI Appendix*, Figs. S1*B* and S2*A*).

Kinetic properties of TcDH. With *c550* or $K_3Fe(CN)_6$ as electron acceptors, the enzyme showed a pH optimum around 9.5 (Fig. 1), matching the pH of the habitat of the host organism. The pH dependences are bell-shaped with the apparent pK_as of ∼8.1 to 8.9 for the acidic and ∼10.2 to 10.9 for the alkaline sides, respectively. When using $K_3Fe(CN)_6$ as an electron acceptor, the form of pH profile becomes somewhat wider on both sides. The pK_a value for the right side can be tentatively attributed to the deprotonation of the lysine residue found in the enzyme active site, Lys103; that

Table 1. Influence of the copper ions on the TcDH activity

TcDH	Activity, μmol × min^{-1} × mg^{-1}*	Copper content, mole per mole of TcDH subunit†
"As isolated"	0.2 ± 0.05	0.8 ± 0.2
"As isolated" after dialysis	0.007 ± 0.003	0.7 ± 0.2
Cu^{2+}-saturated	10.1 ± 0.6	3.0 ± 0.5
Cu^{+}-saturated	13.6 ± 0.3	4.5 ± 1
Recombinant	0	0
Recombinant Cu^{2+}-saturated	9.4 ± 0.4	2.5 ± 0.2
Recombinant Cu^{+}-saturated	9.9 ± 0.1	5.2 ± 0.5

*The activity was measured with *cyt550* as an acceptor, 25 mM borate buffer, pH 9.5.
†The copper content was determined by ICP-MS.

for the acidic side to the protonation of the catalytic histidine residue, His136 (as discussed further later).

Table 2 presents the kinetic parameters of thiocyanate oxidation catalyzed by "Cu^{2+}- and Cu^{+}-saturated" TcDH in the presence of different electron acceptors. For the reaction with low-molecular-weight electron acceptors, Wurster's blue and $K_3Fe(CN)_6$, as well as with *c550,* the Michaelis constants for thiocyanate measured for "Cu^{2+}-saturated," "Cu^{+}-saturated," and "as-isolated" TcDH are quite similar. That is indirect evidence supporting our hypothesis that the activity of "as-isolated" TcDH is associated with the presence of a small amount of the active protein.

The maximum reaction rate, V_m, for thiocyanate oxidation assayed with both low- and high-molecular-weight electron acceptors showed rather similar values. Therefore, the rate-limiting step of the overall process should be the same irrespective of the type of the electron acceptor used.

Anions capable of forming coordination compounds with copper ions, such as cyanate and cyanide, acted as inhibitors of TcDH. Cyanide was the most potent inhibitor (K_i 1.4 μM), showing a competitive inhibition pattern. The reaction product cyanate bound with about the same affinity as the substrate, thiocyanate, and showed a mixed type of inhibition (K_{ic} 0.9 mM, K_{iu} 1.2 mM). Unexpectedly, azide appeared to be a rather weak inhibitor, with an IC_{50} of as high as 60 mM. Other anions tested (nitrate, nitrite, bicarbonate, sulfate, acetate, and iodide) showed no inhibitory effect at 1 mM concentration (thiocyanate concentration was 1 mM, approximately the K_m).

Electron Paramagnetic Resonance (EPR) of TcDH. A concentrated sample of "Cu^{2+}-saturated" TcDH with a copper content of 3.0 (ICP-MS) was studied with EPR spectroscopy. As presented in Fig. 2*A*, the low-temperature X-band spectrum shows a broad, complex signal with at least 11 hyperfine lines. Saturation at 17 K (Fig. 2*B*) sets in at a microwave power of circa −30 dB (0.2 mW), which is not an uncommon value for S = 1/2 Cu^{2+} complexes in proteins. The spectral shape does not change significantly even at high saturation levels (*SI Appendix*, Fig. S5*A*), indicating that individual Cu^{2+} spectra cannot be disentangled by discriminative saturation. The integrated signal intensity as a function of sample temperature (Fig. 2*C*) indicates Curie behavior. The spectral shape also does not change significantly as a function of temperature over a range from 15.7 to 162 K (*SI Appendix*, Fig. S5*B*), indicating that individual Cu^{2+} spectra cannot be disentangled by discriminative temperature-broadening. The spectrum is also found to be essentially independent of pH from pH 6.0 to 9.5 except for a slight further decrease of resolution at high pH (*SI Appendix*, Fig. S5*D*). Quantification versus an external copper standard, assuming noninteracting S = 1/2, gives a spin count of 2.4. To check whether this number may have been affected by the presence of mutual dipolar interaction between the copper ions, we completely denatured the protein with strong acid: the resulting EPR spectrum shows a single, magnetically isolated Cu^{2+} species, doubly integrating to a spin count of 2.8 (*SI Appendix*, Fig. S5*E*).

The only resolving action is partial reduction, e.g., either by redox equilibrium titration or kinetically in the reaction with substrate SCN^- in the absence of an external electron acceptor. A reductive equilibrium redox titration with dithionite of 15-fold diluted enzyme (to obtain enough data points) in the presence of a range of redox mediators (Fig. 2*D*) indicates complex redox behavior. The integrated signal intensity reduces over a much wider potential range than expected for a Nernstian one-electron acceptor. Thus, the Cu ions may have individual reduction potentials that vary over several hundred millivolt; alternatively, the Cu ions may exhibit concerted redox behavior. Indeed, the data can be fit approximatively with a single Nernst curve with a substoichiometric electron value of n = 0.21 (Fig. 2*D*), which possibly suggests significant negative redox cooperativity. At the low-potential end of the titration, the EPR spectrum changes into a shape indicative of an isolated Cu^{2+} ion with $g_{||} \sim 2.3$ and a resolved hyperfine splitting of $A_{||} \sim 130$ G (*SI Appendix*, Fig. S5*C*).

Incubation for 20 min with substrate SCN^- resulted in an EPR spectrum of nearly 60% reduced intensity (Fig. 3), suggesting that this reaction in the absence of the external electron acceptors leads to reduction of two of the three Cu^{2+} ions to Cu^{+}. The process is biphasic: the first spin is reduced quite rapidly, while reduction of the second one requires several minutes under the condition of the experiment. Prolonged incubation affords the isolated Cu^{2+} spectrum also observed at the low-potential end of the redox titration.

For simulation of the spectra, additional data were collected at 35 GHz (Q-band; Fig. 4*A*), and a semiquantitative analysis based on the following assumptions (to keep the problem tractable) was applied: (*i*) it is assumed that the spectrum stoichiometrically represents three copper sites; (*ii*) all EPR parameter tensors are assumed to be axial (e.g., $g_x = g_y \equiv g_\perp$); (*iii*) since an increase in the microwave frequency leads to an increase in the strength of the electronic Zeeman interaction over all other magnetic interactions, we use Q-band (ca. 35 GHz) data to pin down g-values, and these are subsequently used as fixed values in the

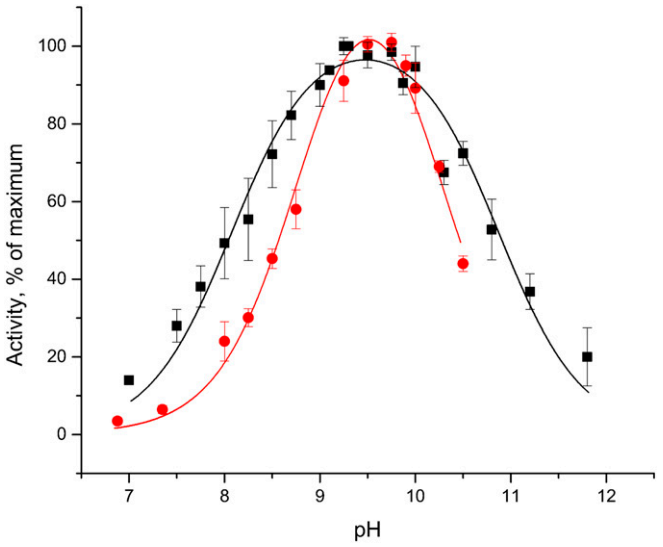

Fig. 1. pH-dependence of the TcDH-catalyzed thiocyanate oxidation with 50 μM *c*550 (red circles) and 1 mM $K_3Fe(CN)_6$ (black squares) as electron acceptors. The activity was measured with 6 mM SCN^- in 25 mM borate buffer (pH 8 to 11.8) and 50 mM Mops (pH 6.8 to 8). The theoretical curves are calculated assuming pK_{a1} of 8.9 and pK_{a2} of 10.2 for *c*550 (R^2 = 0.988 red line) and pK_{a1} of 8.1 and pK_{a2} of 10.9 for $K_3Fe(CN)_6$ (R^2 = 0.962, black line).

Table 2. Kinetic parameters of enzymatic thiocyanate oxidation in the presence of various electron acceptors

	Acceptor					
	Wurster's blue		$K_3[FeCN_6]$		*cyt*550	
TcDH	K_m, mM	V_m, μmol × min^{-1} × mg^{-1}	K_m, mM	V_m, μmol × min^{-1} × mg^{-1}	K_m, mM	*V*m, μmol × min^{-1} × mg^{-1}
As isolated	*	*	*	*	0.9 ± 0.3	0.28 ± 0.03
Cu^{2+}-saturated	0.8 ± 0.1	12.7 ± 0.5 (11.0)	1.2 ± 0.1	11.8 ± 0.8 (10.3)	1.0 ± 0.1	10.2 ± 0.2 (8.9)
Cu^{+}-saturated	0.7 ± 0.1	13 ± 0.2 (11.3)	1.0 ± 0.1	15.4 ± 0.5 (13.4)	1.3 ± 0.2	12.1 ± 0.3 (10.5)
Recombinant Cu^{+}-saturated	*	*	0.8 ± 0.1	12.5 ± 0.4 (10.9)	1.2 ± 0.1	10.0 ± 0.2 (8.7)

Value of $V_m/[E]_0$ (s^{-1}), k_{cat}, is given in parenthesis, where $[E]_0$ is the total enzyme concentration in solution.
*Not determined.

X-band simulation; (*iv*) simulation of the X-band spectrum is inspected in second derivative mode as a higher-sensitivity check on hyperfine pattern; (*v*) the final fit of the overall spectrum is compared to a fit to the spectrum of partially reduced enzyme; and (*vi*) a mixed-valence [Cu(I)-Cu(II)] pair is assumed not to be present, since such a system would give a single S = 1/2 spectrum and this would imply a total copper S = 1/2 EPR stoichiometry of 2 (Fig. 4). The fitting parameters are listed in *SI Appendix*, Table S3, in which the three copper sites are arbitrarily labeled A, B, and C.

In summary, reasonable fits are obtained for the EPR of oxidized TcDH containing three coppers, with consistency between X-band and Q-band data. One species (Cu-C) is unusual; it has the parallel hyperfine splitting, $A_{||}$ = 60 to 80 G, of a blue, type-I copper, although it does not have the coordination, nor the strong color, of a blue copper species. It is reminiscent of the so-called "type-zero" pseudotetrahedral site that is obtained from azurin after mutation of the cysteine ligand into an aspartate and mutation of the methionine ligand into a noncoordinating amino acid (26, 27). The other two species (Cu-A and Cu-B) exhibit EPR parameters that are common for O,N coordinated copper. In the reaction with potassium thiocyanate (KSCN) species, Cu-A is the last one to get reduced.

Three-Dimensional Structure of TcDH. To determine the three-dimensional structure of TcDH and reveal details of the active site architecture, we obtained crystals of both the native and recombinant protein, which differed in the method of activation, crystallization conditions, and the number of copper ions located in the active site of the enzyme (Table 3). The X-ray diffraction data sets were collected at 1.45-Å (TcDH1), 1.6-Å (TcDH2), 1.8-Å (TcDH3), and 1.7-Å (TcDH4) resolution (Table 3 and *SI Appendix*, Tables S4 and S5).

All of the structures but TcDH4 are very similar, with RMSDs between Cα atoms in the range of 0.26 to 0.58 $Å^2$. The TcDH4 structure, the enzyme "as prepared," containing less than one copper ion, reveals conformational changes and double conformations of the active site residues. The structures obtained differ in the number of copper ions in the enzyme active site dependent on the mode of enzyme activation and crystallization conditions. If the enzyme is activated with Cu^{2+} ions (TcDH1), only two coppers are usually found in the active site in the crystal structure. To ensure consistent incorporation of the complete set of three copper ions, the enzyme was activated with Cu^{+} and additional treatment of the protein crystals with Cu^{+} was required (*SI Appendix*). However, under these conditions, extra copper ions with

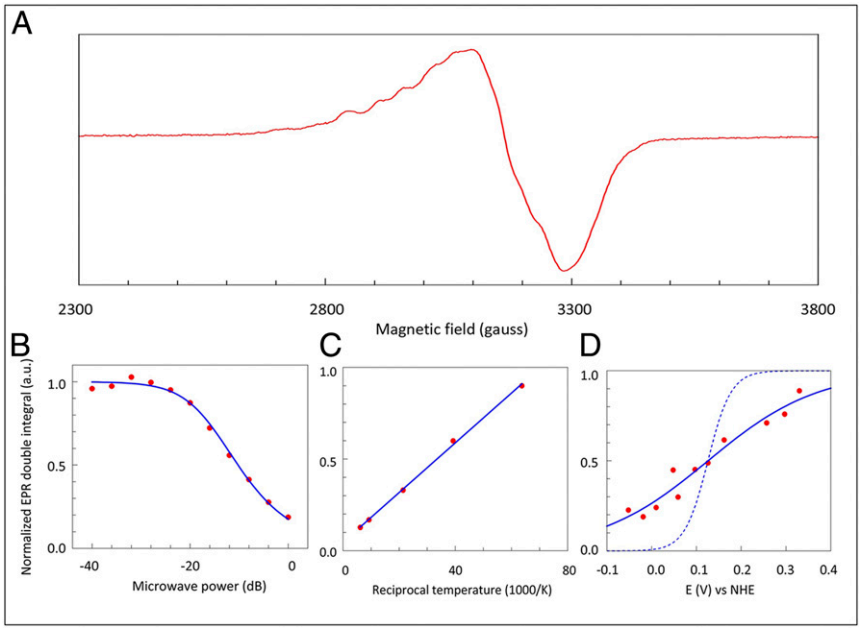

Fig. 2. EPR spectroscopy of TcDH. Wild type TcDH loaded with three coppers. (*A*) Spectrum at 9.3871 GHz and 15.7 K showing a complex pattern of hyperfine lines. (*B*) Microwave-power saturation plot at 17 K shows regular Cu^{2+} saturation. (*C*) Plot of intensity versus reciprocal temperature shows normal Curie behavior. (*D*) Reductive titration by stepwise addition of sodium dithionite shows complex behavior possibly indicative of negative redox cooperativity. Electron stoichiometry with n = 1 (dotted line) or n = 0.21 (solid line). *Materials and Methods* includes detailed experimental conditions.

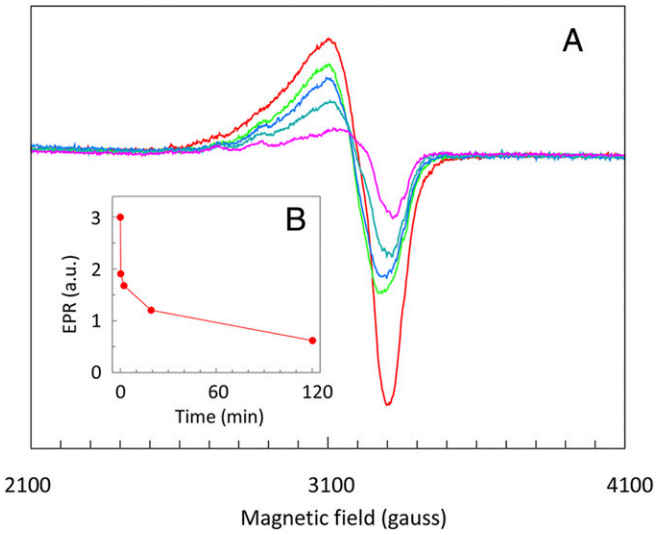

Fig. 3. EPR spectra of TcDH after incubation with the substrate SCN^- in the absence of external electron acceptors. (*A*) EPR spectra of 0.29 mM wild-type TcDH with three coppers, incubated with 1 mM KSCN, taken at time 0 s, 15 s, 2 min plus 15 s, 20 min, and 2 h. (*B*) Course of the reaction presented as double integral of the EPR spectra versus time. The reaction consists of two distinct phases: after 20 min, the initial intensity is reduced by 60%, suggesting reduction of two of the three Cu^{2+} to Cu^+; on a much longer time scale, the third Cu^{2+} also (partially) reduces. Note that the final spectrum is similar, if not identical, to the mononuclear Cu^{2+} spectrum observed at the low-potential end of the redox titration in Fig. 2. EPR conditions: frequency, 9,410 MHz; power, −32 dB; temperature, 17.5 K.

low occupancy (0.5 to 0.2) are found on the protein surface and even at the enzyme active site (TcDH2, TcDH3).

Overall structure of TcDH. Residues 82 to 548 (hereafter, the numbering of residues is given according to the numeration of the complete polypeptide chain derived from the gene sequence), with the exception of the first three residues, 79 to 81, were located in an electron density map. The TcDH molecule is a homodimer with the dimensions of 40 × 40 × 100 Å (Fig. 5*A*). According to the PISA server (28), the surface area of the TcDH dimer is about 28,620 $Å^2$, and the buried area of the subunit is 2,590 $Å^2$. The dimer is consolidated via 30 hydrogen bonds. Approximately 25 of the 70 residues at the dimer interface form hydrophobic contacts with residues of the adjacent subunit. The TcDH molecule displays a seven-bladed beta-propeller topology (B1 to B7; *SI Appendix*, Fig. S6). The blades of the propeller are formed by antiparallel β-sheets (Fig. 5 *A* and *B*). The enzyme active site is located in a cylindrical cavity (8 Å in diameter) in the center of the enzyme subunit (Fig. 5*B*). The C-terminal helix plugs the bottom of the cavity and places the C-terminal residue of the polypeptide chain, Thr548, into the vicinity of the active site. The negatively charged thiocyanate ion enters the active site through the opening of the central cavity. No other substrate and product transport pathways were found.

Active site. Electron density maps revealed up to three copper ions (Cu1, Cu2, and Cu3) in the central cavity formed by the beta-propeller. This region of the structure is considered to be the enzyme active site (Fig. 5 *C*–*E*). The active site includes (*i*) copper ions, (*ii*) residues coordinated to these copper ions (for the Cu1 ion, His206, His381, and Asp314; for the Cu2 ion, His135, His528, and Lys103, the latter residue being coordinated to the Cu2 ion in only one of two possible positions; and for the Cu3 ion, His437 and His482), (*iii*) residues that are not directly coordinated to copper ions but are involved in the formation of a hydrogen bond network or hydrophobic interactions in the active site (Phe436, Lys103), (*iv*) residues involved in the activation of a reacting water molecule W1 (His136 and Glu288), and (*v*) water molecules, including an attacking water molecule W1, and ions from the crystallization media (acetate ion in the TcDH1 structure). All of the active site residues, 11 altogether, are conserved in the closest homologs of TcDH (identity >49%) and form a characteristic template that can be used for mapping potential TcDHs in the metagenomes (24).

The interpretation of the electron density in the TcDH active site as copper ions is unequivocally supported by the strong anomalous signals observed on density maps (*SI Appendix*, Fig. S7). The copper ion Cu1 is present in all of the structures, including the structure of the "as-isolated" enzyme (TcDH4). The occupancy of the copper ion Cu1 is 0.4 for the TcDH4 structure and 1.0 to 0.8 for the other structures (Table 3). It seems reasonable that Cu1 is the copper ion that is mostly retained during the isolation and purification of TcDH and is not removed by exhaustive dialysis. The copper ion Cu2 also has a high occupancy and was found in all TcDH structures activated by copper ions (Fig. 5 *C*–*E*). The copper ion Cu3 was present only in the structure of TcDH2 treated with Cu^+ (Fig. 5*D*) and also had a nearly full occupancy. Failure to achieve complete reconstitution of the enzyme active site with Cu^{2+} ions under crystallization conditions is not surprising. For example, copper is incorporated into laccase crystals only in the form of Cu^+ (29, 30). It is generally assumed that that Cu^+ incorporates into the proteins better because of the difference in solvation shell of +2 and +1 ions. It should also be noted that, in the particular case of TcDH, the coordination of Cu3 copper site favors Cu^+ oxidation state; that of Cu1 and Cu2 sites, Cu^{2+}.

The copper ions Cu2 and Cu3 were not found in the structure of "as-isolated" TcDH (Cu3 is completely absent, while Cu2 has the 0.1 occupancy in just 50% of the subunits). Apparently, the Cu2 and Cu3 coppers are the labile ions that are mostly lost during isolation and purification of the enzyme and can be removed by exhaustive dialysis. Intensive treatment of the protein crystals with Cu^+ ions to facilitate copper incorporation (*SI Appendix*, *Materials and Methods* includes the details of crystallization) into enzyme active site resulted in the binding of extra copper ions to TcDH molecule. Up to two surface-bound copper ions with low occupancy (0.2 to 0.4) are located in the TcDH2 structure in the vicinity of His411 and His309 residues, with water molecules completing their coordination spheres. TcDH3 structure also reveals His411 as a potential surface copper binding site. The same residues, His411 and His309, are also the binding sites for Pt in the TcDH Pt-derivatives. Moreover, a copper ion with an occupancy of ∼0.5 coordinated to His136 is found in the enzyme active site in TcDH2 (Cu4, Fig. 4*D*). We consider this extra copper binding site normally occupied by the conservative water molecule W1 (as detailed later) as an artifact of the copper incorporation procedure not related to the enzyme catalytic activity. Thus, structural studies show some extra unspecific copper binding in the case of Cu^+ activation and are in accord with the observations of Cu^+ binding in excess of 3.0 moles per mole of TcDH subunit recorded by metal analysis (Table 1).

The Cu1 ion is coordinated by His206, His381, and Asp314 and two water molecules (in the TcDH1 structure, one of the water molecules is replaced by an oxygen atom of the acetate ion from the crystallization solution) and has a square pyramidal coordination geometry (Fig. 5*C*). The Cu2 ion has two possible positions in the TcDH structure. In the dominant position (TcDH1, TcDH2), the Lys103 amino group is not coordinated to Cu2 (the distance between the Cu ion and the NZ atom of Lys103 is >3.2 Å) but is involved in a hydrogen bond network, including a hydrogen bond with the catalytically important residue Glu288. In the other position (60 to 70% occupancy in TcDH3), Cu2 is coordinated by His135, His528, Lys103 (the distance between the Cu ion and the NZ atom of Lys103 is 2.6 to 2.8 Å), and two water molecules. The different positions of Cu2 may arise from its different redox states in the final structures, as Cu^{2+} and Cu^+ prefer quite different

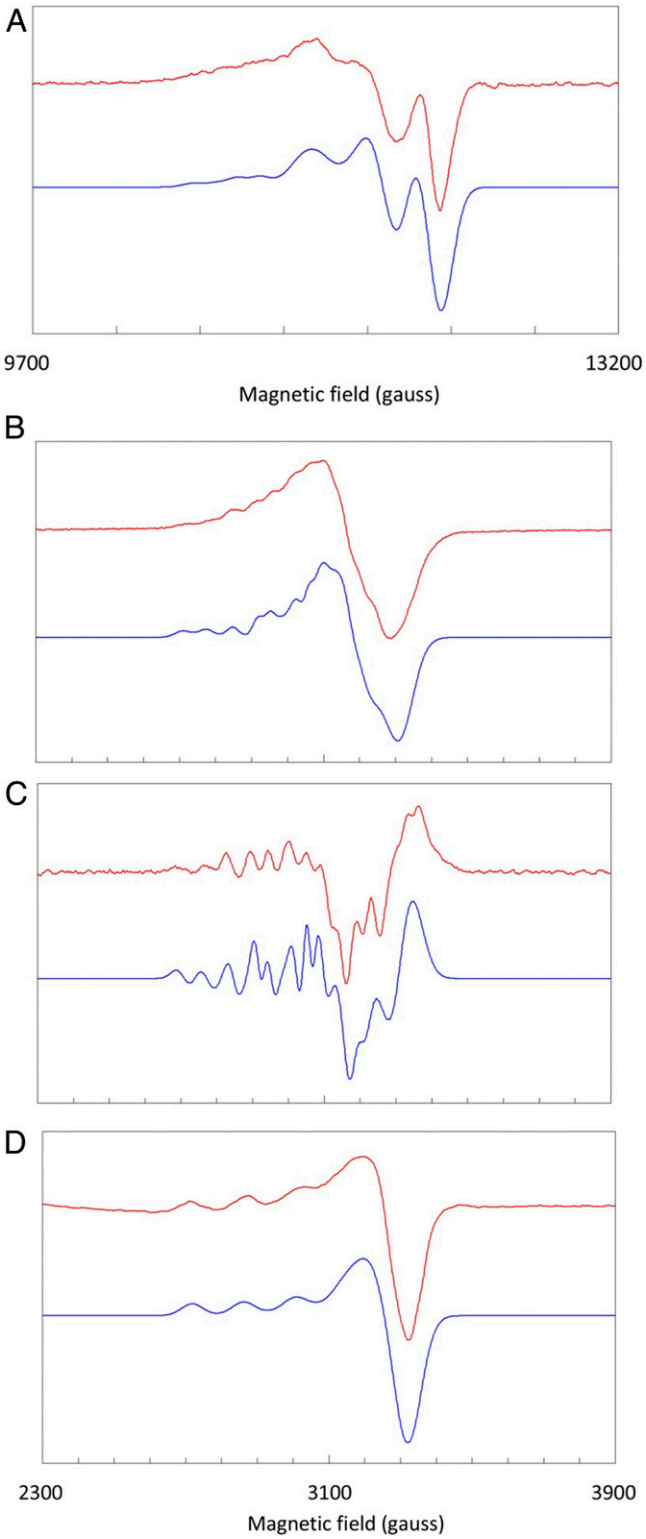

Fig. 4. Simulation analysis of TcDH EPR spectra. Red traces are experimental; blue traces are simulations. (*A*) Q-band spectrum (10 times averaged) taken with settings as follows: microwave frequency, 34.9173 GHz; microwave power, −16 dB of 50 mW; temperature, 10 K. (*B*) X-band spectrum as in Fig. 3*A*. (*C*) Second derivative of *B*. (*D*) X-band spectrum (16 times averaged) of TcDH incubated with 1 mM KSCN for 120 min; settings as follows: frequency, 9.4162 GHz; power, −36 dB of 200 mW; temperature, 20 K. *SI Appendix*, Table S3 A and B provides simulation parameters.

coordination environments. Reduction of the metal centers under the X-ray beam is a well documented phenomenon (reviewed in ref. 31; see also a later work, ref. 32). Both Cu2 positions, with and without coordination bond with Lys103, were considered in the modeling of the molecular reaction mechanism (as detailed later).

In the TcDH2 structure, the Cu3 ion is coordinated by two histidines (His437 and His482; Fig. 5*D*). No Cu3 was observed in the structure of TcDH3, in which one of the ligands of the copper ion, His482, was mutated to a glutamine residue, irrespective that the enzyme was activated with Cu^{+} ions under the same protocol as TcDH2 (Fig. 5*E*). The overall architecture of the TcDH active site was retained on this mutation.

A conservative water molecule W1 is observed in TcDH3 (Fig. 5*E*). In this structure, it forms hydrogen bonds with His136 and Glu288 and is an evident candidate for a nucleophilic particle that may participate in the enzyme catalytic mechanism. A water molecule in the same position is also located in TcDH4, the "as-prepared" enzyme structure. In the structure of TcDH1, the position of W1 is occupied by an oxygen atom of the acetate ion; in TcDH2, by a nonspecifically bound copper ion, Cu4, coordinated by His136.

In the active site, copper ions form a near-isosceles triangle. The base of the triangle in TcDH2 is formed by Cu2 and Cu3 copper ions, at a distance of 5.1 Å. The distance between Cu1 and Cu3 ions is 6.1 Å, and that between the Cu1 and Cu2 ions is 6.2 Å. The distance from the active site (from Cu2) to the protein surface is ∼9 Å, which allows for direct electron transfer from active-site copper ions to the external acceptor. The EPR data show that the copper ions do not electronically interact with each other. Altogether, TcDH reveals a previously unknown active site architecture containing three copper ions. A three-copper cluster of TcDH can be regarded either as a completely new copper center or as a novel combination of three mononuclear copper sites functioning in a concerted mode.

It is tempting to reconcile the data obtained from EPR and structural studies and attribute individual EPR signals revealed in the course of modeling to the particular copper ions. EPR signal of type C can be tentatively assigned to Cu3, because this is the only copper ion with a special coordination sphere different from coordination modes of Cu1 and Cu2 and resembling a so-called type-zero pseudotetrahedral copper (figure 1 in ref. 27). EPR data show that two copper ions undergo reduction in the TcDH active site in the presence of the substrate. We can assume that these are Cu2 and Cu3 because of their close proximity to each other, facilitating electron exchange with the substrate molecule. In this case, EPR signal of type A can be related to Cu1, because this is the last copper center to undergo reduction both under single turnover conditions and in the course of redox titration. Finally, EPR signal of type B should be attributed to Cu2.

Comparison of TcDH and N_2O-reductase, N_2OR. The seven-bladed beta-propeller scaffold is a common structural motif that is known to harbor various active sites performing quite different chemistries. In particular, it has been observed in at least two other types of Cu enzymes, namely galactose oxidase [PDB ID 1GOF (33)] and the catalytic subunit of N_2OR [PDB ID 2IWF (34) and 3SBQ (7)]. The structural similarity of TcDH and the catalytic subunit of N_2OR, containing the so-called CuZ [4Cu:2S] cluster, is particularly striking (*SI Appendix*, Fig. S8). While sequence alignment hardly reveals any similarity that does not exceed 24%, structural alignment based on the structures of TcDH2 (6UWE) and N_2ORs from *Shewanella denitrificans* (5I5M), *Achromobacter cycloclastes* (2IWF), and *Pseudomonas stutzeri* (3SBQ) shows that these structures can be superimposed with RMSDs of 2.15 to 2.27 $Å^2$. The structural alignment places the CuZ cluster of N_2OR in the vicinity of the TcDH active site close to Cu2–Cu3 copper ions (*SI Appendix*, Fig. S8). The CuZ center of N_2OR is coordinated by seven histidine residues, the same number of histidines that are present in the characteristic template of TcDH and participate in copper binding. Five out of seven histidine residues of TcDH,

Table 3. TcDH structures discussed in this work

Structure	TcDH source	Resolution, Å	PDB ID	Method of activation	Occupancy of copper ions			Notes
					Cu1	Cu2*	Cu3	
TcDH1	Wild type	1.45	6I3Q	Cu^{2+}	1.0	(1) 0.8	—	Acetate ion (two possible positions) located in active site
TcDH2	Recombinant	1.6	6UWE	Cu^{+}	1.0	(1) 0.9	0.9	An additional copper ion with 0.4 to 0.5 occupancy in enzyme active site; surface copper ions with low occupancy, 0.5 to 0.2
TcDH3	Recombinant	1.8	6SJI	Cu^{+}	0.8	(1) 0.3–0.4, (2) 0.7–0.6	—	His482Gln mutant; His482 is the ligand of Cu3
TcDH4	Wild type	1.7	6G50	"As isolated"	0.4	(1) 0.1	—	Double conformations of the active site residues

*The copper ion Cu2 in the TcDH structures has two positions: position 1, in which the amino group of Lys103 is not involved in the Cu2 coordination, and position 2, in which the amino group of Lys103 is involved in the coordination of Cu2.

residues 135, 136, 381, 437, and 528 can be roughly superimposed on the related histidine residues of N_2ORs.

However, a closer look at the two structures reveals substantial differences in the mode of spatial organization of their active sites. In the CuZ cluster, the maximum/minimal distance between copper ions is 3.4/2.58 Å (Cu-Cu bond is 2.48 Å), while the two closest coppers in TcDH (Cu2 and Cu3) are within 5.1 Å distance from each other. Seven histidines in N_2OR are clustered within a close range to each other, providing, together with bridging S-atoms, a coordination environment to the compact CuZ copper cluster. In TcDH, the same seven histidines are spread over much wider space, coordinating three individual copper ions

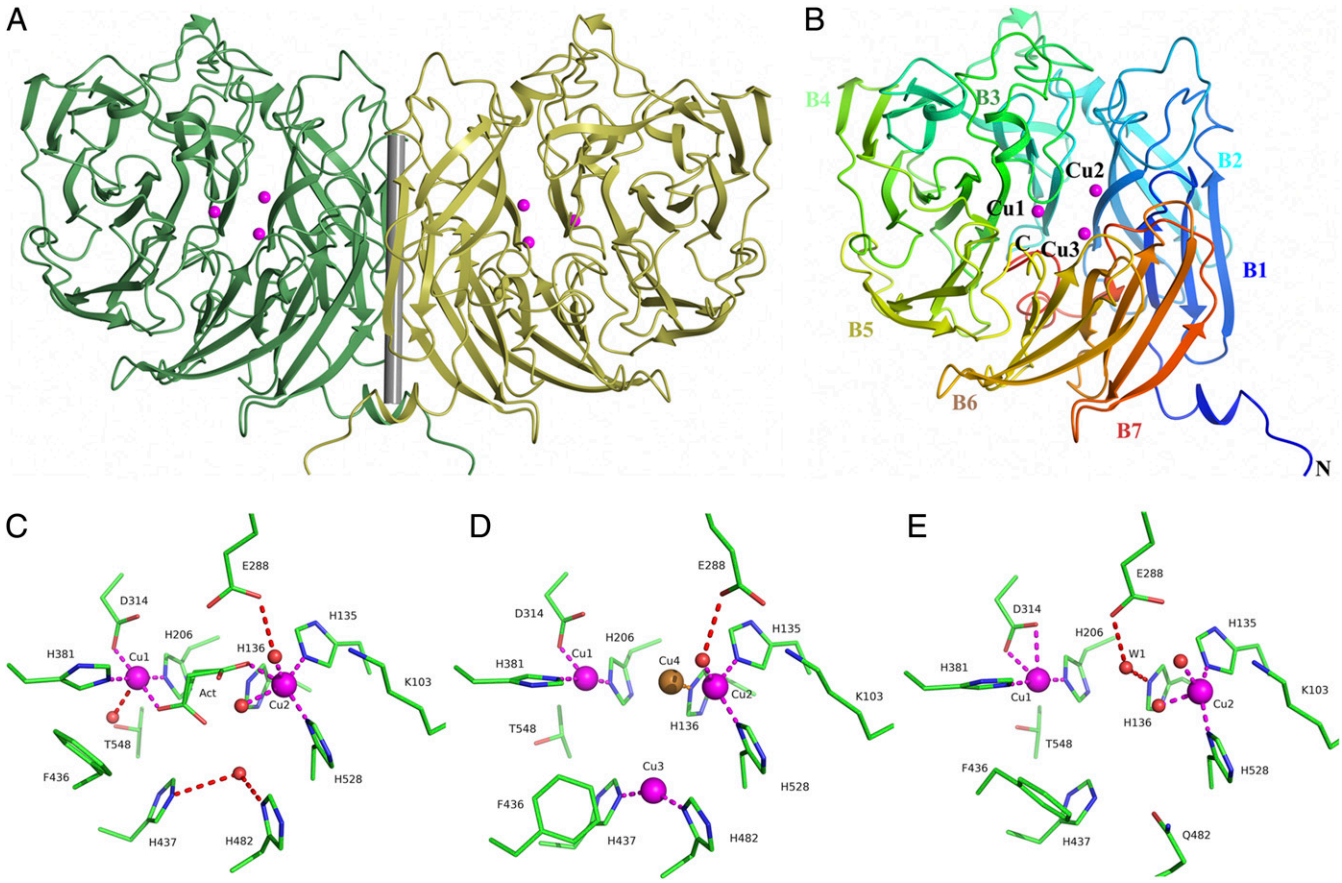

Fig. 5. Structure of TcDH. (*A*) Structure of the TcDH dimer. The TcDH monomers are represented by green and gold ribbon models. The noncrystallographic twofold axis is shown as a gray cylinder. (*B*) Ribbon model of the TcDH monomer. The opening of the active-site cavity is located in front of the figure. Color blend is applied through the model by amino acid number. Copper ions are in magenta. Blades of the propeller structure are numbered B1 through B7. (*C*) The structure of the active site of TcDH1 containing two copper ions. The protein residues, solvent molecules, and two possible positions of the acetate ion (Act) with 0.5 occupancy each are represented as ball-and-stick models colored by atom type. (*D*) The structure of the active site of TcDH2 containing a complete set of three copper ions. Copper ions 1 to 3 are represented by magenta and low-occupancy Cu4 ion by gold spheres. (*E*) The structure of the active site of TcDH3 (His482Gln mutant) with a catalytic water molecule W1 shown as a red sphere. Only one position of the Cu2 ion is indicated. The coordination and hydrogen bonds are indicated by dashed lines in magenta and pale crimson, respectively.

positioned well apart from each other (six histidine residues), while one histidine, His136, is assumed to play a critical role in the enzyme catalytic mechanism, acting as an acid–base catalyst.

Another major difference between TcDH and N_2OR is that TcDH activity, that is its active site, can be recovered just by adding copper ions, while it is well known that N_2OR activity cannot be reconstituted in vitro, and incorporation of CuZ cluster requires participation of a set of genes organized in a special *nos* operon (35, 36). *Tv. paradoxus* genome contains an operon (*nosRDFYZL*) coding for N_2O-reductase (NosZ), which is very similar to known N_2ORs, and auxiliary proteins, NosYDF(R), required for protein maturation. The gene coding for TcDH belongs to a distinct region of genome containing, in the case of *Tv. paradoxus*, a specialized set of genes assumed to participate in copper trafficking (24, 37). Proteins coded by these genes may assist in the final assembly of copper ions into the TcDH in the periplasm.

Despite the close similarity of the fold, TcDH and N_2OR seem to be quite dissimilar enzymes with differently organized active sites. The three-copper cluster of TcDH could by no means be a degenerated part of the CuZ cluster. Thus, TcDH and N_2OR provide another example of how nature grafts different catalytic configurations (in this case copper clusters) on the conservative spatial scaffolds (β-propellers).

Site-Directed Mutagenesis. In the TcDH structure, His136 and Gln288 residues are located in the active site within an H-bonding distance to the conservative water molecule W1 that can function as a nucleophile in the course of the enzyme catalytic turnover. To confirm the role of His136 and Glu288 in the catalysis, we replaced both residues with alanine in recombinant TcDH to abolish the ability of these residues to accept protons. Both "as-isolated" TcDH mutants (Glu288Ala and His136Ala) were inactive and remained inactive after standard activation procedures using either Cu^{2+} or Cu^{+}. However, the mutant forms of the enzymes retained Cu-binding capacities and were able to bind up to 4.0 ± 0.2 Cu atoms into the protein, as demonstrated by metal analysis.

A possible functional role of His136 in catalysis is further confirmed by the observed pH-dependence of the enzyme catalytic activity (Fig. 1). As expected, the protonation of the catalytic residue His136 at low pH values should diminish its ability to abstract a proton from the water molecule, resulting in enzyme inactivation. Thus, the observed pK_a of ∼8.1 to 8.9 can be tentatively attributed to His136.

In summary, His136 and Glu288 can act as typical acid–base catalysts by accepting two protons during the TcDH catalytic cycle, increasing the nucleophilicity of the attacking water molecule.

His482, one of the two ligands of Cu3, was mutated to Gln. The mutated enzyme was devoid of catalytic activity and revealed the presence of only two copper ions, Cu1 and Cu2 (TcDH3), thus further supporting the crucial role of Cu3 in enzyme functioning.

Putative Molecular Mechanism of Catalysis by TcDH. Several lines of evidence point to a putative position of thiocyanate in the active site of TcDH. EPR data show that two copper ions of the enzyme active site undergo reduction during catalytic turnover. The best guess, as discussed earlier, is that these are Cu2 and Cu3 copper ions. Thus, the sulfur atom of the substrate that undergoes oxidation in the course of the chemical reaction should be positioned in the vicinity of these ions, forming an apex of the S–Cu2–Cu3 triangle. Cu1 that does not undergo a redox change in the catalysis is the most evident candidate to coordinate the nitrogen atom of thiocyanate.

If we position the substrate molecule in this way with its N terminus facing Cu1, a conservative water molecule W1 (Fig. 5*E*) will be able to act as a nucleophilic agent and attack the carbon atom of the substrate. This water molecule in the structure of TcDH3 active site is located at a hydrogen-bonding distance from His136 (2.7 to 2.8 Å) and Glu288 (2.7 to 2.9 Å). The two protons of W1 that are released during catalytic turnover can be accepted by the imidazole moiety of His136 and the carboxyl group of Glu288. Moreover, one of these residues may abstract a proton from the water molecule already in the initial step of the enzyme-catalyzed reaction, producing a much stronger attacking nucleophile, a hydroxide ion.

Quantum mechanics/molecular mechanics (QM/MM) modeling. We extended the study with the combined quantum mechanics/molecular mechanics simulations to propose a mechanistic explanation of the experimental data and further verify and detail the proposed molecular mechanism of the primary reaction in the active site of TcDH: the nucleophilic attack of the SCN^- by a water molecule.

We started with verification of the QM/MM protocol used in the present work. The TcDH1 crystal structure was chosen as the source of coordinates of heavy atoms, and QM/MM calculations were performed at the PBE0-D3/6–31G**/AMBER level of theory. The detailed comparison of the calculated and experimental geometry configurations is presented in *SI Appendix*, Fig. S9 *A–C*. Briefly, the calculated structure correctly reflects all of the important features, the 3D structure of the entire protein, coordination shells of Cu^{2+} ions, and the spin density distribution. Thus, the suggested protocol can be utilized for the reaction mechanism calculations.

The complete QM subsystem used for modeling comprises 165 atoms and is presented in *SI Appendix*, Fig. S9*D*. We considered a set of models with different orientations of the SCN^- in the active site as well as different protonation states of Lys103. The main criterion from the computational point of view was reasonable values of the energy barriers for all of the elementary steps along the reaction path. The only molecular model that met this criterion is discussed later. In this model, Lys103 has a protonated side chain and does not form a coordination bond with Cu2, and the orientation of the substrate is such that the sulfur atom points toward the Cu2 and Cu3 ions, while nitrogen is coordinated via Cu1, which is in line with both the structural information and the EPR data (Fig. 6*A*). Simulations employing models where Lys103 is deprotonated and coordinates Cu2 resulted in prohibitively large activation barriers. A detailed discussion of the role of the protonation state of Lys103 in catalysis is provided in the *SI Appendix*. In brief, the calculations show that Lys103 coordination to Cu2 prevents shortening of the Cu2–Cu3 distance that occurs in the transition state and is required for C-S bond break (as detailed later). It seems that the formation of the coordination bond between Lys103 and Cu2 displaces the copper ion from the active site and prevents the chemical reaction from proceeding. Thus, the pK_a of ∼10.2 to 10.9 observed on the pH-dependences (Fig. 1) can be ascribed to the deprotonation of Lys103.

Prior to the nucleophilic attack, the catalytic water molecule is activated by His136 that abstracts the first proton to be transferred during catalysis. The C-S bond cleavage occurs in a single step with an energy barrier of 13.9 kcal/mol, which corresponds to a rate constant of 590 s^{-1} at 303 K according to the transition state theory (Fig. 6*A*). The rate constant of the chemical step should be equal to or higher than the overall reaction rate constant k_{cat}. The theoretical estimate for the rate constant of the thiocyanate decay exceeds the observed k_{cat} for the electron acceptors (9 to 15 s^{-1}; Table 2). This suggests that the primary chemical step of the reaction is not rate-limiting in the entire catalytic turnover.

In the transition state (TS), heavy atoms of the substrate and the oxygen atom of the catalytic water molecule lie in a single plane, whereas the hydrogen atom is 48° out of plane. The transition state is stabilized by an additional coordination bond between the sulfur atom and Cu2, resulting from the shortening of the distance between the Cu2 and Cu3 ions from 5.38 Å in the ES structure to 4.46 Å in the TS structure. The following transformations include the proton transfer to the Glu288 residue and C-S bond cleavage. This gives rise to an intermediate with a linear cyanate, which is

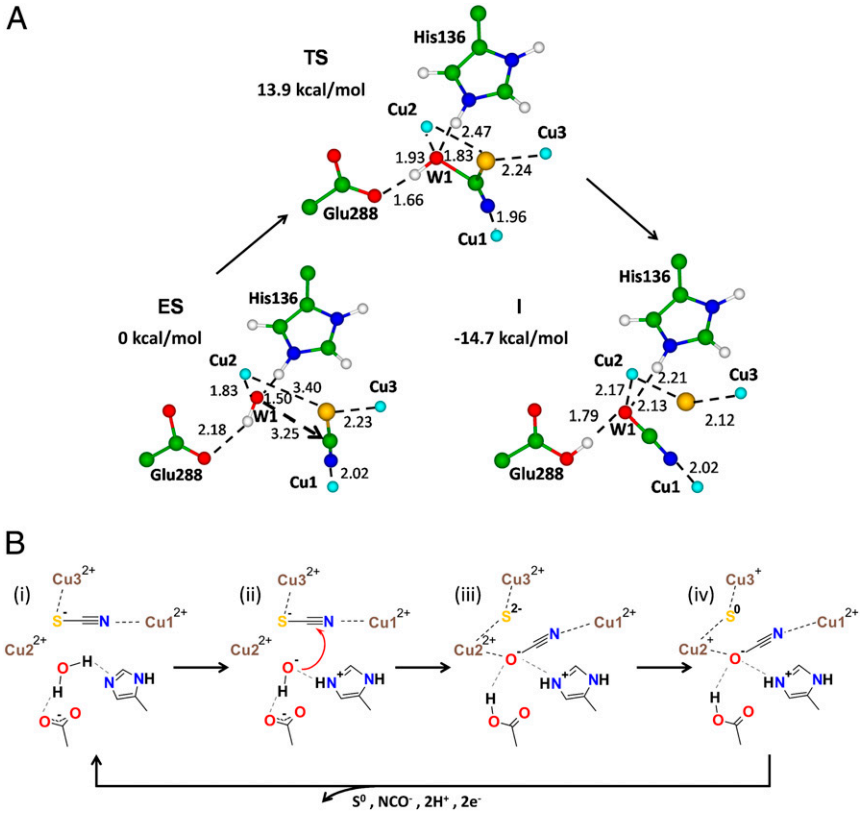

Fig. 6. (*A*) Structures of the reagents (ES), transition state (TS), and the products (I) of the chemical stage of the reaction obtained in QM/MM modeling and relative Gibbs energies of the stationary points. Distances are given in Angstroms. Color code: carbon atoms are in green; nitrogen in blue; sulfur in yellow; oxygen in red; copper in light blue; and hydrogen in white. The coordination and hydrogen bonds are indicated by dashed lines. The distance between the attacking water molecule W1 and the carbon atom of the substrate is indicated by the dashed arrow. (*B*) The entire reaction mechanism of a thiocyanate hydrolysis by TcDH.

14.7 kcal/mol stabilized compared to the ES complex. A sulfide anion (S^{2-}) coordinates the Cu2 and Cu3 copper ions, and the cyanate is located between the Cu1 and Cu2 ions. The suggested mechanism requires only minor displacements of the nonhydrogen atoms during the formation of the reaction intermediate (I), which is critical for the reaction rate. The transition from the substrate (NCS^-) to the product (NCO^-) can be described as an angular, ~30° movement of the C-N fragment coupled with the cleavage of the C-S bond in the substrate and the formation of the C-O bond in the product, with other atoms roughly preserving their original positions (Fig. 6*A*).

Conclusion

According to the proposed mechanism (Fig. 6*B*), the thiocyanate anion binds to the enzyme active site in such a way that one copper ion coordinates the N atom of the substrate, while the S atom is located between two other copper ions (*i*). The conserved active site histidine and glutamate residues act as bases that abstract two protons from the catalytic water molecule. The first one is transferred to the His136 to form the reactive hydroxide that attacks the central carbon atom of the substrate (*ii*). The C-S bond cleavage and C-O bond formation occur in a single step, and another proton is transferred to the Glu288 to stabilize OCN^- (*iii*). We suggest that the next stage of the catalytic cycle involves the oxidation of the reduced sulfur atom to elemental sulfur through two one-electron transitions and the reduction of Cu2 and Cu3 ions to the oxidation state Cu^+. This assumption is supported by EPR spectroscopy that shows that two of the three paramagnetic centers (Cu^{2+} ions) in TcDH can be reduced by thiocyanate to the diamagnetic Cu^+ state in the absence of the electron acceptor. The reduction is accompanied by a change in the form of the complex original spectrum, which is finally reduced to the isolated Cu^{2+} spectrum, probably originating from Cu1 that retains its original redox state (*iv*). In the final step, still to be elucidated, electrons are transferred from the two Cu^+ ions to the external electron acceptor, either independently or via some preferred route (e.g., Cu2 → Cu3 → acceptor); cyanate, sulfur, and two protons are released from the enzyme; and the native active site is restored. According to the stationary kinetic data, the overall rate-limiting step of the enzyme catalytic turnover occurs either at stage (*iii*) or (*iv*) and is the same both for low- and high-molecular-weight electron acceptors.

To summarize, we have discovered and characterized an enzyme, thiocyanate dehydrogenase, with a special multimetal site consisting of three coppers in a triangle configuration, catalyzing an unpreviously reported reaction of converting thiocyanate to cyanate and elemental sulfur without participation of molecular oxygen.

Materials and Methods

Bacterial Strains and Growth Conditions. Three *Thioalkalivibrio* strains were cultured in batch mode on a mineral sodium carbonate-bicarbonate medium containing 0.6 M total Na^+, pH 9.75, as described previously (21). Thiocyanate (10 to 15 mM) was used as an energy and nitrogen source. The standard mineral medium used to grow the *Thioalkalivibrio* strains contained 5 μg/L Cu^{2+} in the form of EDTA complex. Extra copper was supplied in the form of citrate complex. The concentration was varied from 0 to 400 μg/L in growth experiments aimed at confirming the essential role of copper ions in the growth of *Tv. paradoxus* (ARh1) and *Tv. thiocyanoxidans* (ARh2 and ARh4) with thiocyanate. The biomass growth was monitored by the increase in

OD_{600}, and thiocyanate utilization was assessed by the colorimetric assay based on the formation of $Fe(SCN)_3$ (2).

Isolation, purification, and characterization of TcDH. TcDH from *Tv. paradoxus* ARh1 was purified from the cells grown on thiocyanate with the addition of an extra 30 μg/L Cu^{2+} to the standard medium. A periplasmic cell fraction was used as a source of TcDH. The purification procedure included two steps, anion exchange chromatography and size exclusion chromatography. The purity of TcDH was assessed by SDS/PAGE. Recombinant TcDH of the wild-type (recTcDH) and mutant forms were obtained in *Escherichia coli* expression system. Detailed description of the expression and purification of native TcDH, recTcDH, and the mutants His136Ala, Glu288Ala, and His482Gln is provided in *SI Appendix, Materials and Methods*.

The TcDH activity was assessed using 6 mM thiocyanate and 50 μM horse heart cytochrome *c* (c550; Sigma) as an electron acceptor at 30 °C in 25 mM borate buffer, pH 9.5. The enzyme concentrations in the reaction were ∼100 nM for the "as-isolated" enzyme and ∼10 nM for the Cu^{2+}- and Cu^{+}-saturated enzyme. The activity (micromole per minute per milligram) was calculated from the steady-state rate of c550 reduction, which was measured spectrophotometrically at 550 nm ($\varepsilon_{550} = 22.5\ mM^{-1}cm^{-1}$). The activity was calculated as the average of three measurements.

A standard "Cu^{2+}-saturated" TcDH was prepared by incubation of the enzyme at a concentration of 0.6 mg/mL (∼10 μM) with a 200-μM $CuCl_2$ solution in 25 mM borate buffer, pH 9.5, for 2 h, followed by dialysis overnight against two changes of 25 mM borate buffer, pH 9.5. "Cu^{+}-saturated" TcDH was prepared in a similar way but with the addition of a mixture of $CuCl_2$ and sodium ascorbate in a 2:1 ratio (the TcDH–to–total Cu ratio was 1:20) to a solution of TcDH. This Cu-to-ascorbate ratio was experimentally determined to be that at which the maximum activity of TcDH was achieved.

Substrate and Product Assays. The thiocyanate concentration in the reaction was analyzed by a colorimetric assay in the form of $Fe(CNS)_3$ (38). Cyanate, as a reaction product of thiocyanate degradation by TcDH, was measured spectrophotometrically at 310 nm after reaction with 2-aminobenzoic acid (39).

The elemental sulfur reaction product was analyzed by reversed-phase HPLC on a Nucleosil 100–5C18 column [25 cm × 3.2 mm (i.d.)] equilibrated with MeOH:H_2O (90:10) as previously described (25). The biosulfur produced by *Tv. paradoxus* during growth with thiocyanate or thiosulfate was used as a reference compound (*SI Appendix*, Fig. S4).

EPR spectra were collected on a Bruker ECS-106 X-band spectrometer with a home-built helium-flow cooling system. The sample was 15.1 mg/mL (as determined from absorption at 205 and 280 nm) and contained 3.0 Cu ions (0.69 mM in total copper) as determined with ICP-MS after overloading followed by dialysis of excess Cu. The buffer was 25 mM borate, pH 9.5. Typical EPR conditions were as follows: microwave frequency, 9.39 GHz; microwave power, −36 dB (50 μW); modulation frequency, 100 kHz; modulation amplitude, 8 G; temperature, approximately 16 K. The fit to the power plot (Fig. 2*B*) is a saturation curve under the assumption of heterogeneous broadening: $EPR = 1/\sqrt{[1 + (10E0.1P/10E0.1P_{0.5})]}$ in which P is the power in −dB and $P_{0.5}$ is the power at 50% saturation, $P_{0.5} = -15$ dB. The temperature plot (Fig. 2*C*) was determined from 15.7 K (−36 dB) to 162 K (−16 dB). EPR intensity is the second integral of the complete spectrum normalized for variable settings of electronic gain and microwave power. The fit is a straight line. Spectra corresponding to limiting values of employed power, temperature, and redox potential are shown in *SI Appendix*, Fig. S5. Simulation parameters from the analysis of the EPR spectra by spectral simulation (Fig. 4) are presented in *SI Appendix*, Table S3. The redox titration procedure has been described in detail in ref. 40.

Q-band data were taken on a Varian E-line Q-band spectrometer with a home-built helium flow system. Spectra were recorded in rapid-passage mode with the bridge switched to dispersion detection, with subsequent numerical differentiation.

Crystallization and Preparation of Heavy-Atomic Derivatives. Crystallization experiments were performed using "Cu^{2+}-saturated" (TcDH1) and "as-isolated" (TcDH4) TcDH from *Tv. paradoxus* ARh1 and "Cu^{+}-saturated" recombinant TcDH (TcDH2 and TcDH3; Table 3). The X-ray diffraction datasets were collected at 100 K at the European Synchrotron Radiation Facility (ESRF) at the ID23-1, ID29, and ID30B beamlines (Grenoble, France). The structure of TcDH1 was solved by single-wavelength anomalous dispersion (SAD) using its Pt derivative. The other structures were solved by the molecular replacement method using the TcDH1 structure as the starting model. Detailed information about TcDH crystallization and structure determination is presented in *SI Appendix, Materials and Methods* and Tables S4 and S5.

Molecular modeling. We prepared several molecular models. Some were used to validate the QM/MM protocol applied throughout this study, while the other, e.g., of the enzyme–substrate complex, were employed to study the reaction mechanism. The details of the construction of the models are discussed in the *SI Appendix*.

System solvation and preliminary relaxation was performed in a classical molecular dynamics (MD) approach in the NAMD program package (41). The ES complex was solvated in a rectangular water box 80 × 80 × 90 $Å^3$ in size and neutralized with sodium ions. The MD run was performed in NPT ensemble at 300 K with a 1-fs integration time step. The protein molecule and ions were described with the CHARMM36 (42) force field; the SCN^- substrate with the CGenFF force field (43). The MM minimization without any constraints was followed by the 1-ns MD run, keeping protein atoms fixed to obtain proper solvation shell. For further QM/MM simulations, the water box was reduced to the total size of the system equal to 10,656 atoms. All QM/MM calculations were performed in the NWChem program package (44). The MM subsystem was treated with the AMBER force field (45). The QM subsystem comprised the substrate SCN^-, three Cu^{2+} ions, and their coordination shells including His135, His206, Asp314, His381, His437, His482, and His528; and the catalytic His136 and Glu288, other residues that form hydrogen bonds in the active site (Lys103, Gln156, Asp529, Arg544), and six water molecules, including the catalytic one: 165 atoms in total, including link atoms (*SI Appendix*, Fig. S9*D*). The density functional theory method was applied to describe the QM part with the PBE0 hybrid functional with the empirical dispersion correction D3 and the 6–31G** basis set for all atoms including copper. No restraints or constraints were imposed on the model system upon the stationary points search. The multiplicity of the systems containing three copper ions was set to 4 (three spins of 1/2 from Cu^{2+} ions). We checked whether the wave function obtained reproduces correctly the localization of the unpaired electrons. All stationary points were confirmed by calculations of the Hessian matrix. Conventional formulae of the statistical thermodynamics with the harmonic oscillator and rigid rotor approximations were utilized to add thermal and entropic contributions at 30 °C.

ACKNOWLEDGMENTS. We thank Prof. Gideon Davies (Univ. of York), Prof. Michael Blackburn (Univ. of Sheffield) and Prof. Alexander Gabibov (Inst. of Bioorganic Chemistry of Moscow) for critical reading the manuscript and valuable remarks and suggestions. We thank Dr. Konstantin Polyakov for his invaluable help with the structural part of the work. We thank the staff of ESRF and personally Dr. Alexander Popov for assistance and support in using beamline ID23-1 and Dr. Konstantin Boyko of the Research Centre of Biotechnology for valuable discussions. MALDI-TOF-MS and ICP-MS analyses were carried out on the equipment of the Shared-Access Equipment Centre "Industrial Biotechnology" of the Federal Research Center "Fundamentals of Biotechnology," Russian Academy of Sciences. QM/MM calculations were performed using the equipment of the shared research facilities of high-performance computing resources at Lomonosov Moscow State University. Funding: D.Y.S. was supported by Russian Foundation for Basic Research Grant 19-04-00401 (microbiological experiments), while the other Research Centre of Biotechnology members were supported by Russian Science Foundation Grant 14-24-00172 (protein purification, biochemical characterization, crystallization and structural work). G.M. was supported by the European Research Council Advanced Grant PARASOL (No. 322551).

1. E. I. Solomon *et al*., Copper active sites in biology. *Chem. Rev.* **114**, 3659–3853 (2014).
2. A. Messerschmidt, "Copper metalloenzymes" in *Comprehensive Natural Products II: Chemistry and Biology*, H.-W. Liu, L. Mander, Eds. (Elsevier Science, 2010), vol. 8, pp. 489–545.
3. N. J. Robinson, Structural biology: A platform for copper pumps. *Nature* **475**, 41–42 (2011).
4. N. Vita *et al*., A four-helix bundle stores copper for methane oxidation. *Nature* **525**, 140–143 (2015).
5. S. V. Antonyuk, C. Han, R. R. Eady, S. S. Hasnain, Structures of protein-protein complexes involved in electron transfer. *Nature* **496**, 123–126 (2013).
6. R. Balasubramanian *et al*., Oxidation of methane by a biological dicopper centre. *Nature* **465**, 115–119 (2010).
7. A. Pomowski, W. G. Zumft, P. M. Kroneck, O. Einsle, N_2O binding at a [4Cu:2S] copper-sulphur cluster in nitrous oxide reductase. *Nature* **477**, 234–237 (2011).
8. D. C. Brady *et al*., Copper is required for oncogenic BRAF signalling and tumorigenesis. *Nature* **509**, 492–496 (2014).
9. F. Tisato, C. Marzano, M. Porchia, M. Pellei, C. Santini, Copper in diseases and treatments, and copper-based anticancer strategies. *Med. Res. Rev.* **30**, 708–749 (2010).
10. S. Cosnier, M. Holzinger, A. Le Goff, Recent advances in carbon nanotube-based enzymatic fuel cells. *Front. Bioeng. Biotechnol.* **2**, 45 (2014).
11. S. V. Antonyuk, R. W. Strange, G. Sawers, R. R. Eady, S. S. Hasnain, Atomic resolution structures of resting-state, substrate- and product-complexed Cu-nitrite reductase provide insight into catalytic mechanism. *Proc. Natl. Acad. Sci. U.S.A.* **102**, 12041–12046 (2005).
12. K. Brown *et al*., A novel type of catalytic copper cluster in nitrous oxide reductase. *Nat. Struct. Biol.* **7**, 191–195 (2000).

13. B. Bissaro *et al*., Oxidative cleavage of polysaccharides by monocopper enzymes depends on H_2O_2. *Nat. Chem. Biol.* **13**, 1123–1128 (2017).
14. J. A. Lyons *et al*., Structural insights into electron transfer in *caa*3-type cytochrome oxidase. *Nature* **487**, 514–518 (2012).
15. S. Buschmann *et al*., The structure of *cbb*3 cytochrome oxidase provides insights into proton pumping. *Science* **329**, 327–330 (2010).
16. B. Hermann, M. Kern, L. La Pietra, J. Simon, O. Einsle, The octahaem MccA is a haem c-copper sulfite reductase. *Nature* **520**, 706–709 (2015).
17. S. Collado, A. Laca, M. Díaz, Catalytic wet oxidation of thiocyanate with homogeneous copper(II) sulphate catalyst. *J. Hazard. Mater.* **177**, 183–189 (2010).
18. D. P. Kelly, S. C. Baker, The organosulfur cycle: Aerobic and anaerobic processes leading to turnover of C1-sulfur compounds. *FEMS Microbiol. Rev.* **87**, 241–246 (1990).
19. Y. Katayama, T. Kanagawa, H. Kuraishi, Emission of carbonyl sulfide by *Thiobacillus thioparus* grown with thiocyanate in pure and mixed cultures. *FEMS Microbiol. Lett.* **114**, 223–228 (1993).
20. Y. Katayama *et al*., Thiocyanate hydrolase is a cobalt-containing metalloenzyme with a cysteine-sulfinic acid ligand. *J. Am. Chem. Soc.* **128**, 728–729 (2006).
21. D. Y. Sorokin, T. P. Tourova, A. M. Lysenko, J. G. Kuenen, Microbial thiocyanate utilization under highly alkaline conditions. *Appl. Environ. Microbiol.* **67**, 528–538 (2001).
22. D. Y. Sorokin *et al*., *Thioalkalivibrio thiocyanoxidans* sp. nov. and *Thioalkalivibrio paradoxus* sp. nov., novel alkaliphilic, obligately autotrophic, sulfur-oxidizing bacteria capable of growth on thiocyanate, from soda lakes. *Int. J. Syst. Evol. Microbiol.* **52**, 657–664 (2002).
23. T. Berben, L. Overmars, D. Y. Sorokin, G. Muyzer, Diversity and distribution of sulfur oxidation-related genes in *Thioalkalivibrio*, a genus of chemolithoautotrophic and haloalkaliphilic sulfur-oxidizing bacteria. *Front. Microbiol.* **10**, 160 (2019).
24. S. I. Tsallagov, D. Y. Sorokin, T. V. Tikhonova, V. O. Popov, G. Muyzer, Comparative genomics of *Thiohalobacter thiocyanaticus* HRh1T and *Guyparkeria* sp. SCN-R1, halophilic chemolithoautotrophic sulfur-oxidizing gammaproteobacteria capable of using thiocyanate as energy source. *Front. Microbiol.* **10**, 898 (2019).
25. Maxxam Analytics International Corporation for Alberta Environment and Parks, "Development and validation of analytical methods for elemental sulfur in Alberta soils" (Maxxam Analytics International Corporation for Alberta Environment and Parks, Edmonton, Alberta, 2015).
26. K. M. Lancaster, S. DeBeer George, K. Yokoyama, J. H. Richards, H. B. Gray, Type-zero copper proteins. *Nat. Chem.* **1**, 711–715 (2009).
27. K. M. Lancaster *et al*., Outer-sphere contributions to the electronic structure of type zero copper proteins. *J. Am. Chem. Soc.* **134**, 8241–8253 (2012).
28. E. Krissinel, K. Henrick, Inference of macromolecular assemblies from crystalline state. *J. Mol. Biol.* **372**, 774–797 (2007).
29. O. A. Glazunova, K. M. Polyakov, T. V. Fedorova, P. V. Dorovatovskii, O. V. Koroleva, Elucidation of the crystal structure of *Coriolopsis caperata* laccase: Restoration of the structure and activity of the native enzyme from the T2-depleted form by copper ions. *Acta Crystallogr. D Biol. Crystallogr.* **71**, 854–861 (2015).
30. E. M. Osipov *et al*., Incorporation of copper ions into crystals of T2 copper-depleted laccase from Botrytis aclada. *Acta Crystallogr. F Struct. Biol. Commun.* **71**, 1465–1469 (2015).
31. N. Hakulinen, J. Rouvinen, Three-dimensional structures of laccases. *Cell. Mol. Life Sci.* **72**, 857–868 (2015).
32. K. M. Polyakov *et al*., Structural study of the X-ray-induced enzymatic reduction of molecular oxygen to water by *Steccherinum murashkinskyi* laccase: Insights into the reaction mechanism. *Acta Crystallogr. D Struct. Biol.* **73**, 388–401 (2017).
33. N. Ito *et al*., Novel thioether bond revealed by a 1.7 Å crystal structure of galactose oxidase. *Nature* **350**, 87–90 (1991).
34. K. Paraskevopoulos, S. V. Antonyuk, R. G. Sawers, R. R. Eady, S. S. Hasnain, Insight into catalysis of nitrous oxide reductase from high-resolution structures of resting and inhibitor-bound enzyme from *Achromobacter cycloclastes*. *J. Mol. Biol.* **362**, 55–65 (2006).
35. S. R. Pauleta, S. Dell'Acqua, I. Moura, Nitrous oxide reductase. *Coord. Chem. Rev.* **257**, 332–349 (2013).
36. S. R. Pauleta, I. Moura, "Assembly of CuZ and CuA in nitrous oxide reductase" in *Encyclopedia of Inorganic and Bioinorganic Chemistry* (John Wiley & Sons, 2017).
37. T. Berben, C. Balkema, D. Y. Sorokin, G. Muyzer, Analysis of the genes involved in thiocyanate oxidation during growth in continuous culture of the haloalkaliphilic sulfur-oxidizing bacterium *Thioalkalivibrio thiocyanoxidans* ARh 2T using transcriptomics. *mSystems* **2**, e00102–e00117 (2017).
38. B. Sorbo, A colorimetric method for the determination of thiosulfate. *Biochim. Biophys. Acta* **23**, 412–416 (1957).
39. M. Guilloton, F. Karst, A spectrophotometric determination of cyanate using reaction with 2-aminobenzoic acid. *Anal. Biochem.* **149**, 291–295 (1985).
40. P.-L. Hagedoorn, L. van der Weel, W. R. Hagen, EPR monitored redox titration of the cofactors of *Saccharomyces cerevisiae* Nar1. *J. Vis. Exp.* **93**, e51611 (2014).
41. J. C. Phillips *et al*., Scalable molecular dynamics with NAMD. *J. Comput. Chem.* **26**, 1781–1802 (2005).
42. R. B. Best *et al*., Optimization of the additive CHARMM all-atom protein force field targeting improved sampling of the backbone φ, ψ and side-chain $\chi(_1)$ and $\chi(_2)$ dihedral angles. *J. Chem. Theory Comput.* **8**, 3257–3273 (2012).
43. W. Yu, X. He, K. Vanommeslaeghe, A. D. MacKerell, Jr, Extension of the CHARMM General Force Field to sulfonyl-containing compounds and its utility in biomolecular simulations. *J. Comput. Chem.* **33**, 2451–2468 (2012).
44. M. Valiev *et al*., NWChem: A comprehensive and scalable open-source solution for large scale molecular simulations. *Comput. Phys. Commun.* **181**, 1477–1489 (2010).
45. W. D. Cornell *et al*., A second generation force field for the simulation of proteins, nucleic acids, and organic molecules. *J. Am. Chem. Soc.* **117**, 5179–5197 (1995).